

# Ultimate load capacity of unit Strach frames using an explicit numerical method

Kyoungsoo Lee<sup>\*1</sup>, Jung-Wuk Hong<sup>1</sup> and Sang-Eul Han<sup>2</sup>

<sup>1</sup>Department of Civil and Environmental Engineering, KAIST, Daejeon 305-701, Korea

<sup>2</sup>Department of Architectural Engineering, School of Architecture, Inha University, Incheon 402-751, Korea

(Received February 29, 2012, Revised May 29, 2012, Accepted September 24, 2012)

**Abstract.** This study uses an explicit numerical algorithm to evaluate the ultimate load capacity analysis of a unit Strach frame, accounting for the initial imperfection effects of the stress-erection process. Displacement-based filament beam element and an explicit dynamic relaxation method with kinetic damping are used to achieve the analysis. The section is composed of the finite number of filaments that can be conveniently modeled by various material models. Ramberg-Osgood and bilinear kinematic elastic plastic material models are formulated to analyze the nonlinear material behaviors of filaments. The numerical results obtained in the present study are compared with the results of experiment for stress-erection and buckling of unit Strach frames.

**Keywords:** Strach; stress-erection process; bucking analysis; filament element; dynamic relaxation method.

---

## 1. Introduction

As shown in Fig. 1, a Strach system is erected by the so-called “stress-erection” process, in which the tendon is installed in the bottom member by post-tensioning. The overall frame is composed of a non-deformable rigid frame and shape-changing flexible frames, as illustrated in Fig. 2. The structural design and initial stability are determined through this process. The initial imperfections of curvature and excessive yield strain are occurred in the flexible top chord member.

A simply supported boundary condition, consisting of one pin and one roller support, and bottom member details including a sleeve and gap are the main mechanisms enabling the unique properties of stress-erection. Few structural systems exist in which geometry and material nonlinear behavior are more closely tied together than in the Strach system. While an interesting feature, this peculiarity is the one of reason Strach systems have not been reviewed and considered for large-span structures. The pre-existing imperfections of initial curvature and yield strain in the top chord member are not a familiar feature in conventional design methodology.

The previous pioneering research work of Clarke and Hancock (1995) addressed the design methodology of stress frames through comprehensive numerical and experimental studies on the Strach system. They studied the Strach system’s ultimate load capacity analytically by using the

---

\* Corresponding author, Professor, E-mail: [kslee77@kaist.ac.kr](mailto:kslee77@kaist.ac.kr)

implicit finite element method in a two-dimensional formulation considering geometric and material nonlinearity and verified its accuracy by comparing the results with the experimental studies. The design curve of the system was proposed from parametrics studied by using numerical methods. Using this design methodology, Key *et al.* (2000) reported design case studies. It was proven that the system is essentially linear elastic over normal values of working load and approaches the ultimate strength limit state within predicted values after erection.

This paper proposes an explicit nonlinear numerical algorithm for stress-erection and ultimate load capacity analysis, to study the structural behavior and design methods for Strarch system. The initial imperfections induced by the stress-erection process are considered in ultimate load capacity, buckling and post-buckling analysis.

To this end, the explicit solution, the dynamic relaxation method (DRM) with the kinetic damping technique (Lee *et al.* 2011, Rezaiee-pajand and Alamatian 2010, 2011, Alamatian 2012, Rodriguez *et al.* 2011) is used to solve the equilibrium equation using vector equations, without the need for any implicit matrix derivation and operation. Satisfaction of the equilibrium force deformation relationship is required only.

The plastic zone (distributed plasticity or spread of plasticity) method is used to ensure accurate stress distribution in sections of the flexible top chord member. The member is subdivided into several elements along its length and the cross-section to model the material's nonlinearity. In the literature, the material nonlinearity is often evaluated at a fixed number of cross sections of filaments or fibers (Mari 2010). Each section is subdivided into longitudinal filaments with inherent advantages in uniaxial stress-strain behavior from which the behavior of the element section is derived.

The subdivided section modeling methodology is typically divided by the use of displacement-based or flexibility-based elements. The displacement-based subdivided filament beam element derives its stiffness matrix directly from the classical finite element displacement approach (Mari 2010). The disadvantages of this method are problems of numerical instability near or at the ultimate resistance state. The flexibility-based fiber beam-column element was proposed based on the classical displacement-based stiffness method to develop more robust and reliable elements. The stiffness matrix is derived by inverting the flexibility matrix that describes the relationship between force and deformation. The advantage of the flexibility-based fiber beam element formulation stems from the realization that, irrespective of the state of the element, the force interpolation functions always satisfy the equilibrium equations of the element as long as no element loads are applied. In other words, the assumed internal force distributions are exact no matter what material nonlinearities take place at the section level, even as the element starts losing strength when deformed beyond its ultimate capacity.

The distinction between the filament and fiber approaches is not meaningful when the DRM is used because this method does not use a tangent stiffness matrix; only an element force equation is required. For this reason, this study subdivides the element section into displacement-based filament elements (Mari 2010), and the element internal forces are always evaluated by integrating, over the volume of the element, the contribution of each steel filament over the sectional areas within the element. Numerical integration over the element length is performed by Gaussian quadrature using two gauss points.

Correlation studies between analytical results and the experimental response of stress-erection and ultimate load capacity for a unit Strarch frame show the ability of the proposed method to describe the nonlinear behavior of the flexible top chord member in a Strarch frame.

## 2. Description of the starch system

As shown in Figs. 1 and 2, the Starch system is a unique steel structural system capable of a span of 110 m and 87 m before and after construction, respectively, a length that can house a Boeing 747 commercial airplane. The system is divided into rigid and flexible frames by the role of the bottom chord details. A gap and sleeve are introduced to the bottom chord member in flexible section frames, which enable the flexible section to deform almost freely. As a result, the structural design shape and structural stability is determined at the final stage of the stress-erection process. The Starch frame predominantly comprises square and circular hollow section structural steel members, usually welded together into frame segments that are subsequently bolted together on-site into complete frames. However, during the stress-erection process, the curvature and yield strain eventually introduce excessive plastic strain in the top chord member of the flexible section frame. This is the most unusual feature of the system.

To verify the structural ultimate load capacity of a Starch frame to be constructed in Korea for an airplane hangar, experimental studies were performed on the scale unit frame shown in Fig. 2. The height and length of the unit frame are 4.7 m and 7.2 m, respectively, and a gap of 332 mm length is introduced. The top chord member section is subdivided into many filament elements for the numerical study. The element stiffness and forces are evaluated by integrating over the volume of the element. A geometrically nonlinear truss element is used to model the web member, and a gap element is adopted in the bottom member.

## 3. Numerical model

To investigate the gradual yielding in a cross section of the top chord member, a formulation of 3D filament beam elements (Mari 2010) is used to evaluate its geometric and material nonlinear behavior. Fig. 3 illustrates the section, geometry and degree of freedom (DOF) of the displacement-based FE-

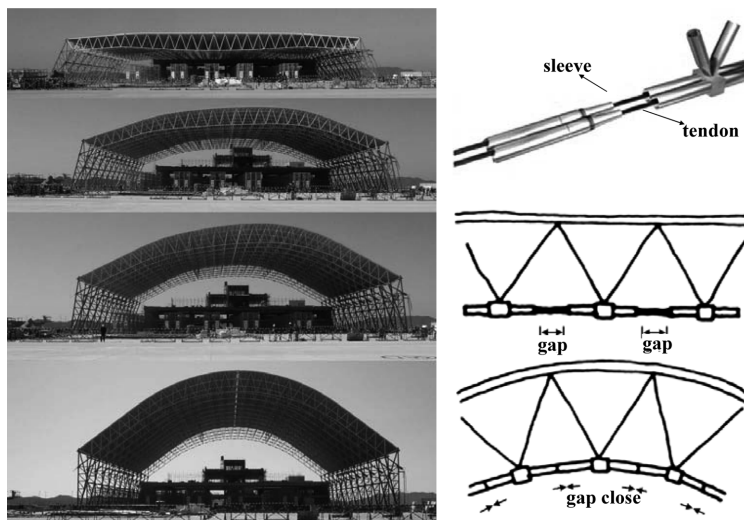


Fig. 1 Erection process and details of the Starch system (Lee and Han 2011c)

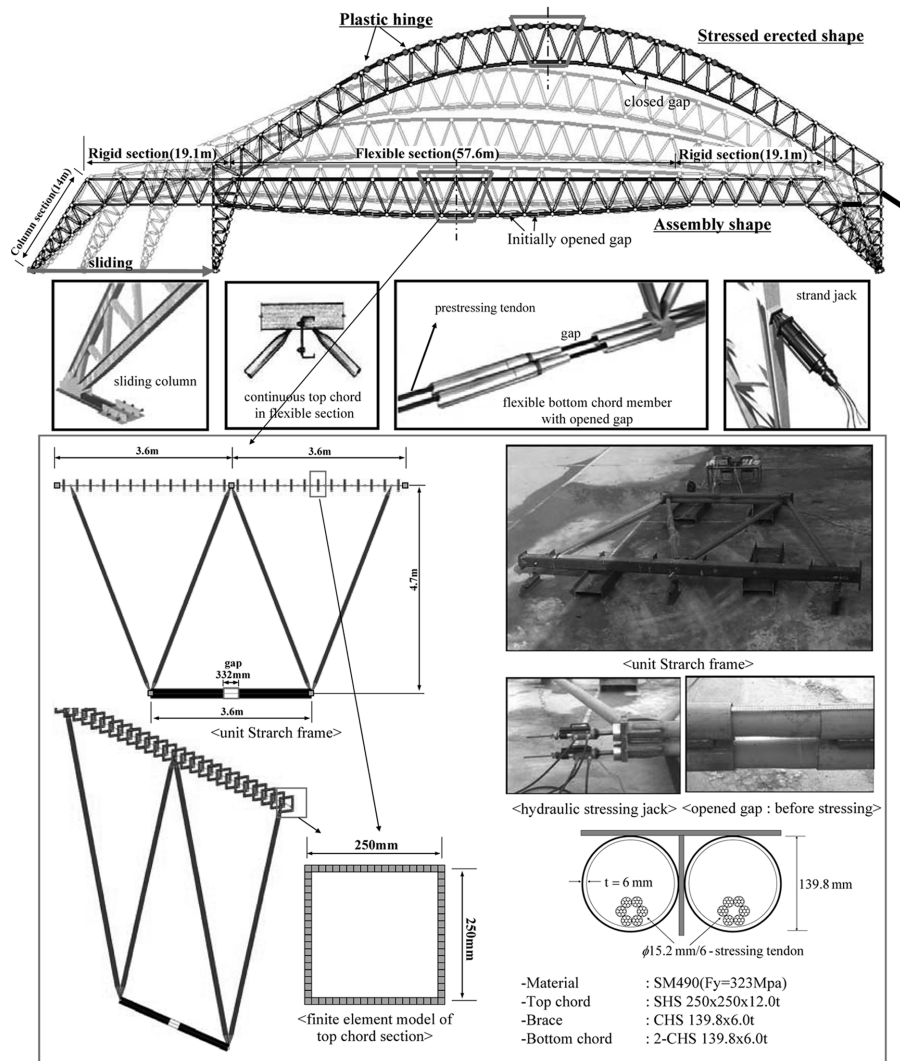


Fig. 2 Starch system and unit model used in this study

formulated filament beam element. The hollow steel section is subdivided into many filament groups. The sectional stiffness and resultant force of each element is evaluated by integrating or summing filaments over the cross-section. The sectional status of material nonlinearity of yielding is evaluated by the uniaxial stress-strain relationship of the material models. Fig. 4 illustrates the material model of this study; the Ramberg-Osgood and bilinear material models are used for the steel filaments. After the uniaxial strain is calculated from the strain-displacement relationship of the element, the current stress of each filament is obtained from the stress-strain curve of the specific material model. The equilibrium status of the system is obtained when the residual force vector is minimized. Therefore, the explicit solution method is sufficiently possible and efficient.

Under these circumstances, the explicit DRM is used to simulate the two stages of the system: the stress-erection process and the ultimate load capacity analysis. The effort required to derive and solve a

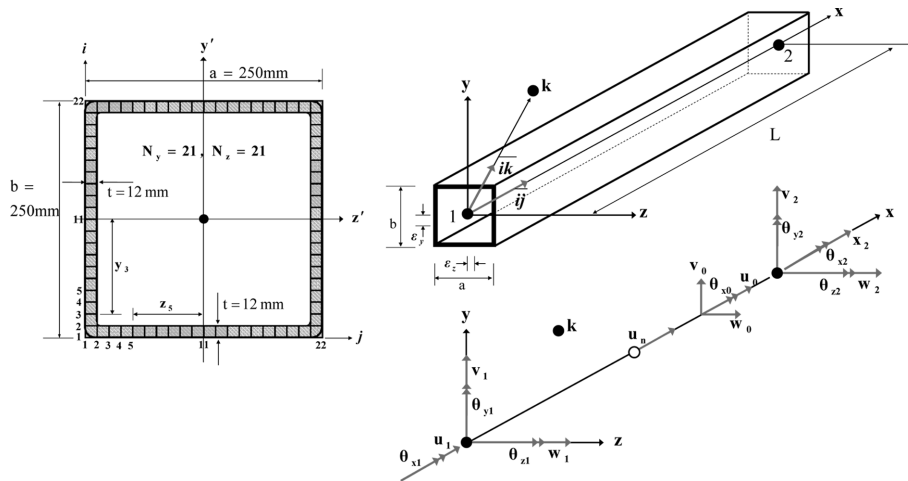
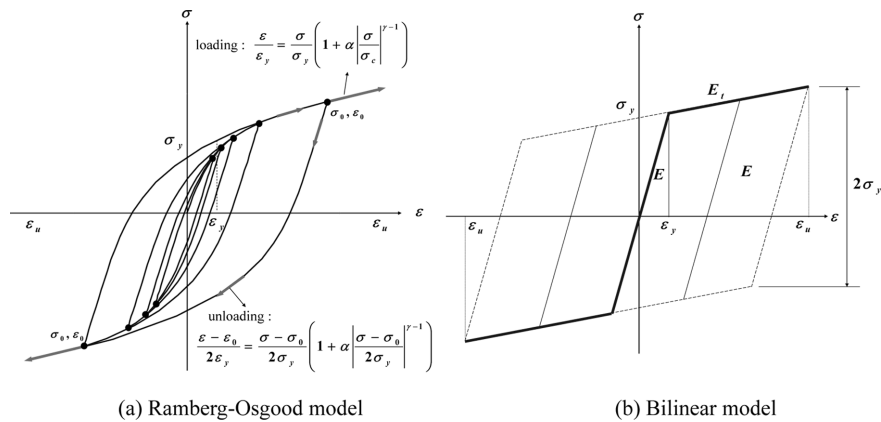


Fig. 3 Filament beam element: section, geometry and degree of freedom



(a) Ramberg-Osgood model (b) Bilinear model

Fig. 4 Uniaxial stress-strain curves of the top chord member

tangent stiffness matrix is omitted by using this quasi-static explicit nonlinear numerical algorithm. Only explicit vector equations are performed to a required degree of accuracy.

### 3.1 Filament beam element

In the FE formulation of displacement-based filament beam elements, the tangent stiffness matrix is derived from the virtual work principle. However, for the explicit algorithm used in this study, the matrix operations of the tangent stiffness matrix are not essential; only the element equilibrium equation of strain-displacement relationship is required. The element nodal force vector is obtained by integrating the stress over the element volume. Because there is no distinction between displacement-based and flexibility-based algorithms, only satisfying the conditions related to the equilibrium equations of the system is necessary. Therefore, the element formulation in this study is identical to that of the flexibility-based algorithm, but the displacement-based algorithm is nevertheless used here to

calculate the strain of the subdivided sectional filaments.

According to the geometry and DOFs of Fig. 3, the displacement fields of the filament beam element on its local  $x$  axis are described as follows.

$$u_0 = N_u u; v_0 = N_v v; w_0 = N_w w; \theta_{x0} = N_\theta \theta \quad (1)$$

here

$$u^T = (u_1, u_2, u_3); v^T = (v_1, v_2, \theta_{z1}, \theta_{z2}); w^T = (w_1, w_2, \theta_{y1}, \theta_{y2}); \theta = (\theta_{x1}, \theta_{x2}) \quad (2)$$

$$N_u = (\psi_1, \psi_2, \psi_3); N_v = (\phi_1, \phi_2, \phi_3, \phi_4); N_w = (\phi_1, \phi_2, -\phi_3, -\phi_4); N_\theta = (\psi_1, \psi_2)$$

In Eq. (2), the shape functions for the Hermitian 13 DOFs are as follows.

$$\psi_1 = 1 - \left(\frac{x}{L}\right); \psi_2 = \left(\frac{x}{L}\right); \psi_3 = 4\left(\frac{x}{L}\right)\left(1 - \frac{x}{L}\right) \quad (3)$$

$$\phi_1 = 1 + 2\left(\frac{x}{L}\right)^3 - 3\left(\frac{x}{L}\right)^2; \phi_2 = 3\left(\frac{x}{L}\right)^2 - 2\left(\frac{x}{L}\right)^3$$

$$\phi_3 = L\left(\left(\frac{x}{L}\right) - 2\left(\frac{x}{L}\right)^2 + \left(\frac{x}{L}\right)^3\right); \phi_4 = -L\left(2\left(\frac{x}{L}\right)^2 - \left(\frac{x}{L}\right)^3\right)$$

An internal midside displacement DOF  $u_n$ , eliminated at the element level, leaves only 12 DOFs for the beam element. This incompatibility in DOFs is necessary for correctly modeling the bending stiffness and to account for shifting of the neutral axis due to cracking and other material nonlinearities in a reinforced concrete beam. For the explicit formulation of this study, only 12 DOFs for the steel beam element are considered without the internal midside displacement DOF  $u_n$ .

The axial displacement  $u_x$  at any point within the beam element can be obtained by assuming Euler-Bernoulli beam kinematics with 12 DOFs as follows.

$$u_x = u_0 - z \frac{dw}{dx} - y \frac{dv}{dx} \quad (4)$$

In Eq. (4),  $u_0$  is a nodal axial displacement omitting the midside  $u_n$  DOF. Thus,  $u_0$  is described as follows.

$$u_0 = N_{u0} u_0 \quad (5)$$

here,  $N_u = (\psi_1, \psi_2); u_0^T = (u_1, u_2)$

The axial strain is then obtained by differentiating  $u_x$  with respect to  $x$ , as follows.

$$\epsilon_x = \frac{du_x}{dx} = \frac{du_0}{dx} - z \frac{d^2w}{dx^2} - y \frac{d^2v}{dx^2} = B_{u0} u - z B_w w - y B_v v \quad (6)$$

The twist  $\varphi$  along the reference axis  $x$  is described as follows.

$$\varphi = \frac{d\theta_{x0}}{dx} = B_{\theta} \theta \quad (7)$$

The uniaxial current stress  $\sigma$  of the subdivided filament elements is then calculated using the relationship of the nonlinear stress-strain curves of the material models given in Fig. 4. Various material models can be used to describe the material nonlinearity of uniaxial stress-strain relationships easily.

An updated Lagrangian formulation, in which the direction of the local reference system is continuously updated as the structure deformed, is used to account for any geometric nonlinearity. The approach is generally used for analyses with large displacements but small strain and incremental rotations. Therefore, the member should be divided along its length of element to be used for the large strain and rotation problems, such as ultimate buckling and post-buckling analysis.

The internal resisting vector or element nodal force vector  $f$  due to the stress  $\sigma$  and torque  $T_x$  in the beam can be obtained by the following equations.

$$f = \int_v B^T \sigma dv + \int_L B_{\theta}^T T_x dx \quad (8)$$

here,  $B = [B_{u0}, B_w, B_v]$

Originally, the formulation of this study was intended to be applicable to 3D problems. However, in this instance, the unit Starch frame is analyzed for the 2D case, and thus, the torque  $T_x$  is not considered.

The advantage of explicit formulation of elements is the possibility of omitting the structural instability of a system matrix and the simplified formulation of element theory. The large numbers of equations used to determine the stiffness of an element are not required, unlike in the more common implicit Newton Raphson (NR) method. The numerical instability of the singularity of a tangent stiffness matrix may occur at a structure's limit state of buckling, causing material yielding and failure. The detection of the structure's critical point is not the subject of this study; otherwise, an implicit algorithm of eigenvalue-based bifurcation analysis would have been used. The explicit formulation of this study is a simple and efficient approach for the simulation of Starch frames during stress-erection and buckling analysis. The accuracy and applicability of these methods are discussed in the following section of the numerical results.

### 3.2 Explicit solution method: dynamic relaxation method

The DRM is a well-known quasi-static iterative nonlinear numerical algorithm, originally proposed by Day (1965). The dynamic motion of a system may be damped into equilibrium due to a viscous or kinetic damping term. Recently, Rezaiee-Pajand and coworkers have proposed remarkable improved numerical algorithm for the optimized DRM with viscous damping technique (Rezaiee-pajand and Alamatian, 2010, 2011, 2012, Rezaiee-Pajand and Sarafrazi, 2010, Rezaiee-Pajand *et al.* 2011).

In contrast, the kinetic damping technique do not use the viscous damping term, which only set the velocity vector to zero when the local kinetic energy peak time step with diagonal mass term. It needs not any formulation of tangent stiffness matrix and implicit solving process. The storage and numerical process of calculating the nodal displacement becomes remarkable simple. The kinetic damping technique was proposed and improved by many researchers (Barnes 1988, Han and Lee 2003, Topping and Iványi 2007, Lee *et al.* 2011, Rodriguez *et al.* 2011, Alamatian 2012) who mainly focused on the simulation of lightweight or unstable structures. However, the DRM with viscous or kinetic damping

techniques is also applicable to buckling or material nonlinear problems (Rezaiee-pajand and Alamatian, 2011, Lee *et al.* 2011).

The Strach system is an unstable structure. It presents a quasi-static problem during the stress-erection process. Thus, the DRM with kinetic damping is appropriate for understanding the stabilizing process of a Strach frame. It is also possible to simulate ultimate buckling and post-buckling analysis of Strach frames without any matrix instability.

The governing equation of the DRM comes from the equation of dynamic systems as follows.

$$p^t = Ma^t + Cv^t + Kd^t \quad (9)$$

Here,  $M$  and  $C$  are a fictitious mass and viscous damping, respectively.  $a^t$  and  $v^t$  are the acceleration and velocity, respectively, at time step  $t$ . The fundamental feature of the DRM is that the static equilibrium state of the structures is determined by the damped motion of the dynamic system during the pseudo quasi-static time integration. It is a static nonlinear method, not a dynamic one. Therefore, the load vector is not time-dependent, but static. Substituting the dynamic load  $p^t$  with the static load  $p$  and rearranging the governing Eq. (9), it can be rewritten as follows.

$$r^t = Ma^t + Cv^t \quad (10)$$

As a result, Eq. (10) is a fundamental governing equation of the DRM. The DRM is an iterative nonlinear algorithm used to find the static equilibrium state of structures by minimizing their total potential energy, and therefore, the left-hand side of Eq. (10) represents an unbalanced force  $r^t$  at a pseudo quasi-static time step  $t$ .

Considering that nodal velocity and acceleration varies linearly for time increment,  $\Delta t$ , the nodal velocity and acceleration can be obtained by using the finite difference method and can be written as follows.

$$v^t = \frac{1}{2} \left( v^{t+\frac{\Delta t}{2}} + v^{t-\frac{\Delta t}{2}} \right) \quad (11)$$

$$a^t = \frac{1}{\Delta t} \left( v^{t+\frac{\Delta t}{2}} - v^{t-\frac{\Delta t}{2}} \right) \quad (12)$$

Substituting Eq. (11) and Eq. (12) into Eq. (10), the unbalanced force can be written as follows.

$$r^t = \frac{1}{\Delta t} M \left( v^{t+\frac{\Delta t}{2}} - v^{t-\frac{\Delta t}{2}} \right) + \frac{1}{2} C \left( v^{t+\frac{\Delta t}{2}} + v^{t-\frac{\Delta t}{2}} \right) \quad (13)$$

Therefore, Eq. (13) can be rewritten in terms of the velocities at times  $t + \Delta t/2$  and  $t - \Delta t/2$  as follows.

$$v^{t+\frac{\Delta t}{2}} = \left[ \frac{1}{\Delta t} M + \frac{1}{2} C \right]^{-1} \left[ \frac{1}{\Delta t} M - \frac{1}{2} C \right] v^{t-\frac{\Delta t}{2}} + \left[ \frac{1}{\Delta t} M + \frac{1}{2} C \right]^{-1} r^t \quad (14)$$

Assuming the viscous damping is only proportional to the mass, the viscous damping becomes as follows.

$$C = \frac{c'}{\Delta t} M \quad (15)$$

where  $c'$  is damping coefficient per unit mass and it is constant for whole structure. After substituting Eq. (15) into Eq. (14), then Eq. (14) yields as follows

$$v^{t+\frac{\Delta t}{2}} = Av^{t-\frac{\Delta t}{2}} + Br^t \quad (16)$$

Where

$$A = \left(1 - \frac{c'}{2}\right) / \left(1 + \frac{c'}{2}\right), \quad B = \frac{\Delta t}{2}(1 + A)M^{-1} \quad (17)$$

It is assumed that the diagonal mass matrix is saved in vector form in Eq. (16) and Eq. (17) for the numerical efficiency, since the structural behaviors are determined through the calculation of nodal velocity vectors without formation of tangential stiffness matrix.

In this study, a simpler and more efficient kinetic damping technique is used to control motion without the viscous damping term. The viscous damping term of Eq. (15) set to zero. And resulting structural response of velocity  $v^{t+\Delta t/2}$  at time step  $t + \Delta t/2$  can be derived explicitly using the velocity  $v^{t-\Delta t/2}$  at the previous time step  $t - \Delta t/2$  from Eq.(16).

As a result, the iterative displacement at time  $t+\Delta t$  can be obtained by from Eq. (17), the iterative displacement at time  $t + \Delta t$  can be obtained by linearly interpolating the velocity at time increment  $\Delta t$  as follows.

$$\delta d^{t+\Delta t} = \Delta t v^{t+\frac{\Delta t}{2}} = \Delta t v^{t-\frac{\Delta t}{2}} + \Delta t^2 M^{-1} r^t \quad (18)$$

The unbalanced residual vector  $r^t$  can be re-written with external initial load  $p_0$  and internal force vector  $f^t$  as follows.

$$\delta d^{t+\Delta t} = \Delta t v^{t-\frac{\Delta t}{2}} + \Delta t^2 M^{-1} (\lambda^{t+\Delta t} p_0 - f^t) \quad (19)$$

here,  $\lambda^{t+\Delta t}$  is the incremental load parameter. A conventional load incremental analysis can be performed by increasing the load parameter  $\lambda^{t+\Delta t}$ . The external load of  $p_0$  is not considered when the stress-erection process is performed. Only the increment of tendon force is applied to the Strach frame.

Dynamic relaxation method is a quasi-static iterative nonlinear solution method. The mass matrix in Eq. (19) need not to be the true structural mass. Rather, Barnes (1988) and Topping and Iványi (2007) reported that an optimally assumed fictitious mass that is proportional to the stiffness of the system would increase the numerical stability and convergence speed.

To gaurantee the numerical convergence, the time step should be kept less than the critical time step that proposed by Barnes (1988) as follows.

$$\Delta t \leq \sqrt{2 \left| \frac{M}{K} \right|} \quad (20)$$

From Eq.(20), Lee *et al.* (2011) calculated the fictitious mass by the diagonal tangent stiffness matrix,  $K_{ii}$  and scale parameter  $\lambda$  as follows.

$$M_{ii} = \lambda \frac{\Delta t^2}{2} K_{ii} \quad (21)$$

The important and unique terms to control the convergence of the DRM in Eq. (19) are the diagonal mass matrix with the fixed time step  $\Delta t$ . At the initial stage of preparing the DRM process, the diagonal tangent stiffness matrix  $K_{ii}$  is assembled and stored in a vector rather than matrix form. The mass matrix could be a simple diagonal rather than a consistent mass. The explicit form of Eqs. (19) and (21) implies that the overall analysis could be performed with a vector equation rather than with a matrix.

Recently, Rezaiee-pajand and Alamatian (2010, 2011), Rezaiee-pajand and Sarafrazi (2010), Rezaiee-pajand *et al.* (2011), Alamatian (2012) proposed new fictitious mass matrix for DRM by using the theorem of Gerschgorin which permits to obtain an upper bound to the eigenvalue of the full stiffness matrix  $K$ . Though these approach show improved and good numerical results, the method presents as a disadvantage that it needs at least the calculation of one stiffness matrix. When the diagonal mass matrix is used without full stiffness matrix, the storage and computational efficiency can be reduced remarkably.

Different from Eq. (21) which the fictitious mass is calculated from the diagonal tangent stiffness,  $K_{ii}$ , In this study, to calculate the fictitious mass matrix, the diagonal mass matrix is determined by assembling the each element diagonal fictitious mass matrix,  $m_{ii,dia}$  directly, and it can be written as follows.

$$m_{ii,dia} = \lambda \frac{\Delta t^2}{2} R^T k_{ii} R \quad (22)$$

In Eq.(22),  $k_{ii}$  and  $R$  are element diagonal linear stiffness matrix and element rotational transformation matrix. As mentioned before, the DRM is not dynamic solution algorithm but quasi-static or static algorithm. Thus, the mass in Eqs. (21) and (22) need not to be the true structural mass. The fictitious mass which is proportional to the stiffness is sufficient for increasing the numerical stability and convergence speed (Barnes 1988, Topping and Iványi 2007, Lee *et al.* 2011).

If we assume that the values of  $E$  and  $GJ$  at the mid-length of the frame element represent the average value along its length,  $k_{ii}$  can be obtained explicitly as follows.

$$k_{ii} = \left\{ \frac{EA}{L}, \frac{12EI_z}{L^3}, \frac{12EI_y}{L^3}, \frac{GJ}{L}, \frac{4EI_z}{L}, \frac{4EI_y}{L}, \frac{EA}{L}, \frac{12EI_z}{L^3}, \frac{12EI_y}{L^3}, \frac{GJ}{L}, \frac{4EI_z}{L}, \frac{4EI_y}{L} \right\}^T \quad (23)$$

$$\text{where } EA = \int_s E ds, EI_y = \int_s E \cdot z^2 ds, EI_z = \int_s E \cdot y^2 ds \quad (24)$$

Numerically, the another explicit form of simplified equation for Eq.(22) are also possible which can be expressed either as following equations.

$$m_{ii,min} = \lambda \frac{\Delta t^2}{2} [\min(k_{ii}) \cdot I] \quad (25)$$

$$m_{ii,max} = \lambda \frac{\Delta t^2}{2} [\max(k_{ii}) \cdot I] \quad (26)$$

In Eqs. (22), (25) and (26), the fictitious masses  $m_{ii,dia}$ ,  $m_{ii,min}$ ,  $m_{ii,max}$  are affected by the element linear stiffness matrix and scale parameter  $\lambda$ . Though, these fictitious masses are assumed to different value,

that are all proportional to the stiffness of structure according to the scale parameter  $\lambda$  and the accuracy of solution is not dependent to the different mass formulation. These assumed fictitious masses affect to the convergence speed only.

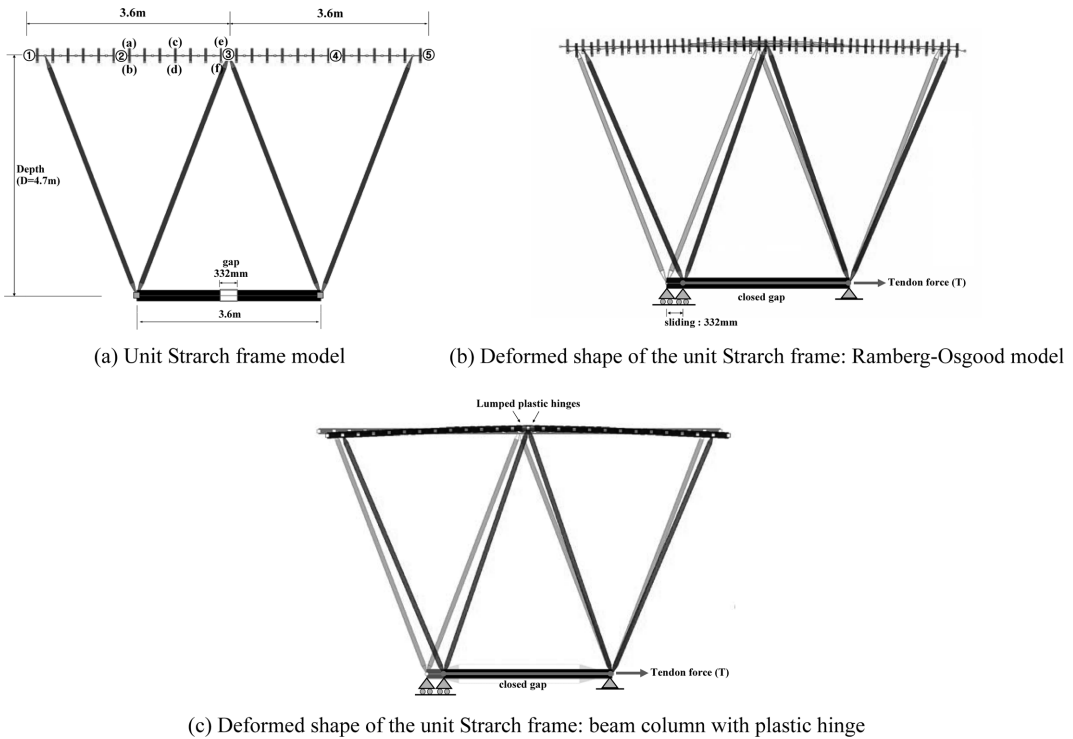
The conditionally stable condition is presented by an explicit algorithm, because it does not use the tangent stiffness matrix. Thus, the numerical processes for maintaining the explicit algorithm's numerical stability and convergence rate should be prepared. To this end, the scale parameter  $\lambda$  of Eqs. (22), (25), (26) is used to control the convergence process. By selecting the optimum value of  $\lambda$ , the system can stably converge to the equilibrium state. A relatively small scale parameter value of  $\lambda$  would make the analysis faster than a larger scale parameter value is used. The scale parameter  $\lambda$  can control the structure's natural period by adjusting the assumed mass matrix. As the value of  $\lambda$  is decreasing, the fictitious mass term is scaled down, and the natural period and required iteration number for convergence decreases as the mass matrix decreases. There is a similar relationship between the mass and the natural period in structural dynamic theory, in which the iteration number for convergence is influenced by the scale parameter  $\lambda$  and the structure's relative natural period. However, if the chosen  $\lambda$  value is too small, the structure's motion may fail to reach the stable convergence state, because a numerical criterion for stability in the explicit algorithm is violated by high speeds or small time increments in the structure's quasi-station motion. Therefore, a larger  $\lambda$  value should be used to find a stable equilibrium state. Since the assumed mass in DRM using the kinetic damping technique is fictitious, the system's calculated period is also fictitious. We can obtain numerical stability in an explicit DRM process by increasing the natural period, because the domain's slow motion will prevent an unstable diverging behavior. In the following section, the effects of different mass formulations and scale parameter  $\lambda$  are discussed.

#### 4. The stress-erection process of a unit strarch frame

A numerical study of the stress-erection process was performed by using the explicit method described in this paper. The unit Strarch frame illustrated in Fig. 2 and Fig. 5 is used for a simulation involving various material models.

The numerical results of this study using the proposed explicit method were compared with a previous analysis using lumped beam-column elements (Lee and Han 2011b) and experimental results, verifying the numerical accuracy and applicability of this method.

Fig. 5 shows the structural characteristics of the Strarch frame. In Fig. 5(a), the gap is opened and the top chord is initially straight. The initial imperfections are not imposed on the frame. As the post-tensioning tendon force in the bottom chord member is increased, the gap closes and the initial curvature and bending strain is imposed. Eventually, after stress-erection, the gap is closed and yield strain is imposed on the top chord member near the joint at ③, not at the joint of ① or ⑤, because of the free boundary condition. In fact, the joints of the top chord are restrained to rotate, as shown in Fig. 2. Therefore, the continuous bending strain is occurred in the top chord member. The tendon force required to erect a Strarch frame is mainly dependent on the self weight of the frame. The amount of strain imposed during installation can be determined by the gap length in the bottom member. The gap length is pre-determined by the catenary shape of the initial Strarch frame. Fig. 5(b) illustrates the deformed shape of the unit Strarch frame obtained using the explicit numerical method with the Ramberg-Osgood material as shown in Fig. 4(a). The requiring control parameter for  $\alpha = 0.4$  and  $\gamma = 5.0$  were used for Ramberg-Osgood material model. Fig. 5(c) shows the result of using a lumped plastic



(c) Deformed shape of the unit Starch frame: beam column with plastic hinge  
 Fig. 5 Unit frame model and deformed shape after the stress-erection process

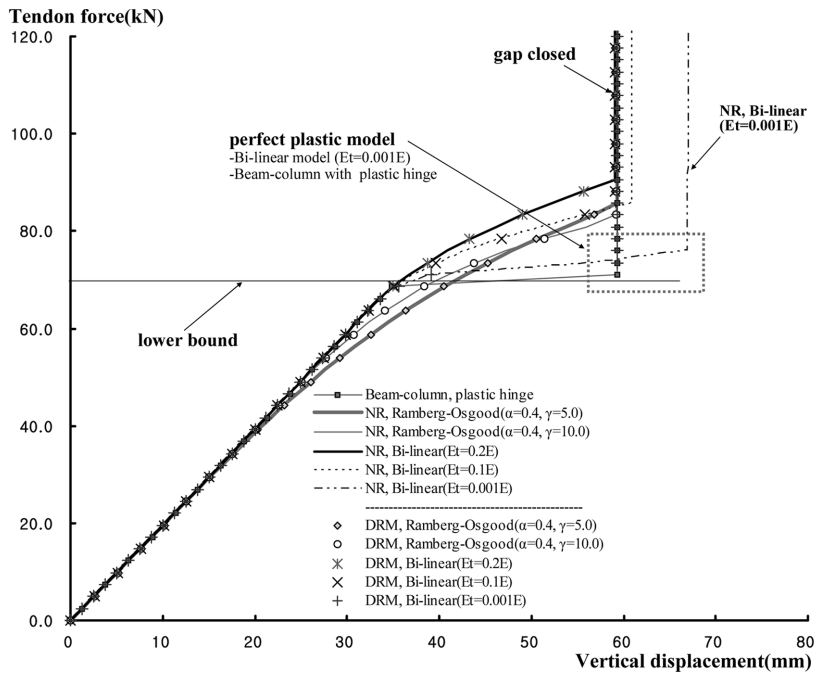


Fig. 6 Tendon force-vertical displacement curves: joint

hinge approach. When the plastic hinge occurred at the joint at , the gap closed suddenly due to the rigid body rotation of that joint. Therefore, the lumped or concentrated deformation and the plastic hinge occurred at the joint.

Fig. 6 illustrates the tendon force-vertical displacement curves at the joint at ③ according to the analytical models with various material control parameters. The resulting curves of this study using the proposed explicit filament elements are in good agreement with the results of the implicit NR method, except in the case of a nearly perfect plastic bilinear model,  $E_t = 0.001E$ . Theoretically, the results of the nearly perfect plastic bilinear model with  $E_t = 0.001E$  are similar to those of the lumped plastic hinge model (Lee and Han 2011b).

In the case of using the bilinear model material model with nearly zero hardening modulus  $E_t = 0.001E$  may represent the perfect plasticity. This means that the analytical value using bilinear model with low hardening modulus are similar to that of plastic hinge model with perfect plastic material model. Even though, the filament beam element uses the section division model for spread of plasticity, according to the nearly perfect plastic model of bilinear model, this filament beam element can be used for perfect plasticity. To illustrate the effects of filament beam element with various hardening modulus,  $E_t$ , we verified the analytical results according the hardening modulus with bilinear model. As decreasing the hardening modulus, eventually the load-deflection curve approach to the plastic hinge model.

The resulting curve obtained by using the implicit NR method with  $E_t = 0.001E$ , a perfect plastic model, shows some errors compared with the other results. The stiffness-based implicit NR method show the quadratic convergence rate when the system is at a normal, stable status. The main shortcoming of this approach is its inability to describe the behavior of the member near its ultimate resistance and after the onset of strain softening. When the yield strain is concentrated at the joint in the perfect plastic model,  $E_t = 0.001E$ , its structural behavior may jump to the next point. Therefore, the tendon force-displacement curve obtained by using NR with a bilinear model of  $E_t = 0.001E$  exceeds the exact solution and is different from the results of the explicit approach.

As shown in Fig. 6, the tendon forces required to erect a unit frame are 71 kN and 73.5 kN using plastic hinge-based beam-column elements and perfect plastic material models, respectively. These tendon forces are approximately 80% of the value of a bilinear model with  $E_t = 0.2E$  and a tendon force of 90 kN. The difference in tendon force values can be attributed to the strain-hardening effects of the material models. And the tendon forces calculated by the analytical models are in good agreement with the predicted lower bound value found in Eq. (28) and experimental value. Fig. 7 presents the deformed shape and resulting filament strain according to the applied material model. As explained before, the resulting strains in the bilinear model with a nearly perfect plastic model are rather concentrated at the joint. However, the strain is gradually spread out over the element length as in the case of Ramberg-Osgood ( $\alpha = 0.4$  and  $\gamma = 5.0$ ) and bilinear models ( $E_t = 0.2E$ ).

Fig. 8 illustrates the effects of scale parameter  $\lambda$  for numerical stability and convergence speed in the case of using Eq. (22) in DRM with kinetic damping technique for this stress-erection problem with bilinear material model ( $E_t = 0.2E$ ). As decreasing the scale parameter  $\lambda$ , the convergence speed is increasing, and the requiring iterations or time steps are reducing. However too small value of  $\lambda = 1$  will make the analysis to be unstable. A relatively small scale parameter value of  $\lambda$  would make the analysis faster than a larger scale parameter value is used. The scale parameter  $\lambda$  can control the structure's natural period by adjusting the assumed mass. As the value of  $\lambda$  is decreasing, the fictitious mass term is scaled down, and the natural period and required iteration number for convergence decreases as the mass matrix decreases. However, if the chosen  $\lambda$  value is too small, the structure's motion may fail to reach the

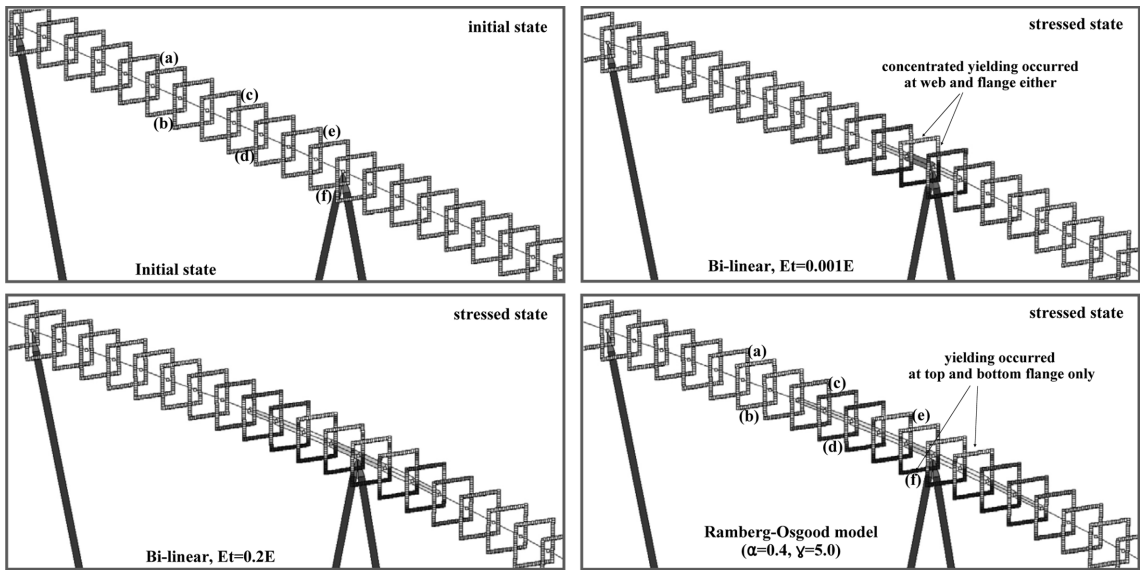


Fig. 7 Deformed shape of the unit frame according to the material model

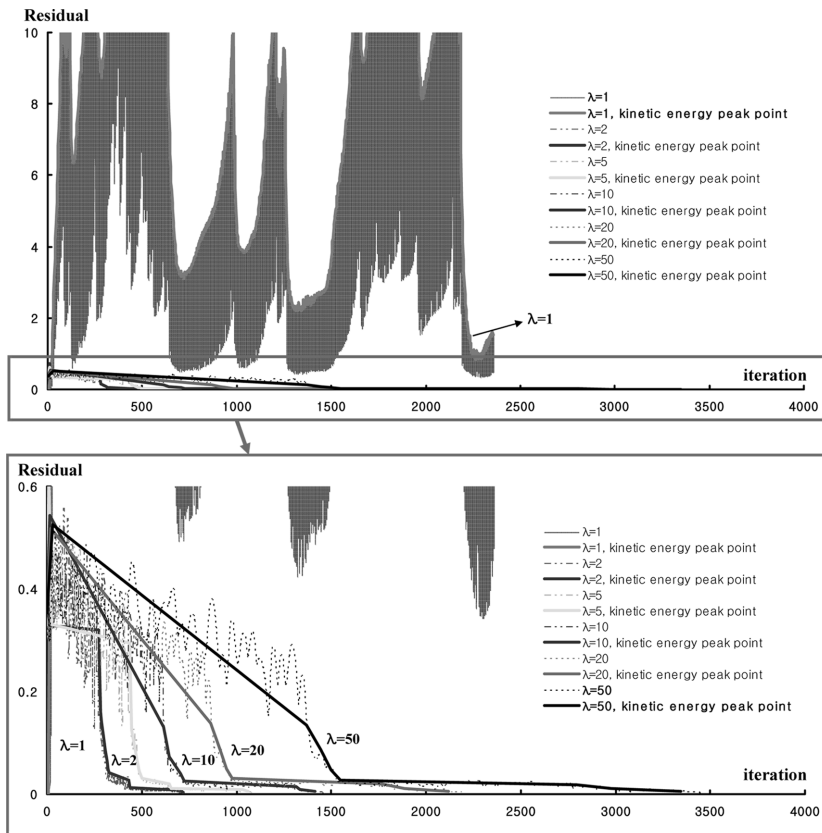


Fig. 8 Convergence process according to the scale parameter  $\lambda$

stable convergence state, because a numerical criterion for stability in the explicit algorithm is violated by high speeds or small time increments in the structure's quasi-station motion.

Therefore, from Fig. 8, it can be said that the optimum value of  $\lambda$  for stable convergence state is  $\lambda = 2$ . This value is also the limit state of numerical stability in this problem. The optimum or limit value of  $\lambda$  is highly dependent on the characteristic (natural period) of structure with the fictitious mass of this study. Rezaiee-Pajand and Alamatian (2010, 2011), Rezaiee-Pajand *et al.* (2011) and Alamatian (2012) have proposed various improved numerical approach for DRM for viscous or kinetic damping method. The reader may refer these papers for further information.

Fig. 9 illustrates the convergence process of various fictitious mass of this study when the Eqs. (22), (25) or (26) are used with scale parameter  $\lambda = 50$ . Usually small value of mass will increase the convergence speed or convergence rate than larger value. In the respect of optimum value of fictitious mass, it can be understood that the minimum diagonal mass  $m_{ii,min}$  of Eq. (25) is the preferable mass. However, too small value of mass may make the analysis to be unstable, as explained before in Fig. 8. Therefore, in this study, the stress-erection process analysis was performed by using the diagonal mass  $m_{ii,dia}$  of Eq. (22) and smallest value of numerical stability,  $\lambda = 2$  for optimum numerical process.

Usually, the initial curvature induced by the stress-erection process exceeds the yield strain or yield curvature of a typical Starch frame. In the case of this study, the yield curvature of the unit Starch frame is  $\kappa_{Yn} = 1.575 \times 10^{-3}$ . The relative ratio of curvature  $\kappa_0/\kappa_{Yn}$  is 1.547 for the Hangar structure in Fig. 2 with an initial curvature  $\kappa_0 = 2.437 \times 10^{-3}$  at its final erected configuration. Consequently, the flexible top chord member may be in a plastic state after erection.

The moment capacity of the top chord member is determined to predict the tendon force required to erect the unit Starch frame. When the strain hardening effect is ignored and the perfect plastic material model is used, the ultimate bending moment  $m_u$  can be substituted with the plastic moment  $m_p$ , which is calculated by a simple equation containing the plastic modulus  $Z$  of the section (SHS-250 $\times$ 250 $\times$ 12t) and the yield stress  $F_y$  (323 MPa) as follows.

$$m_u = m_p = F_y \cdot Z = 328.3 kNm \quad (27)$$

If self-weight of the frames are ignored, the minimum tendon force  $t_{ten}$  and corresponding axial force of the top chord  $p_{top}$  required to close the gap in the bottom chord can be calculated using the following

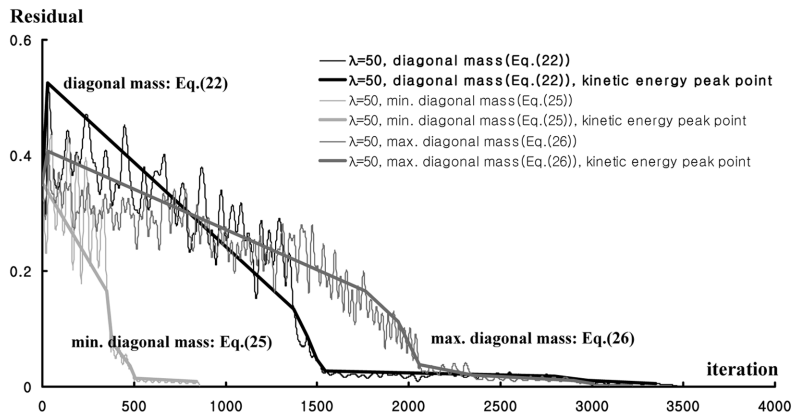


Fig. 9 Convergence process according to the fictitious mass type

simple equation, assuming a statically determinate Strarch frame during the stress-erection process.

$$t_{ten} = -p_{top} = m_u/d \quad (28)$$

Here,  $d$  is the distance between the top and bottom chords. From this simple equation, the tendon force is calculated as 69.8 kN. This is the lower bound of the required tendon force range if the strain hardening effect is ignored. The perfect plastic material model is used, and the self-weight of the frame is not considered. This tendon force value of 69.8 kN is nearly identical to the values of 71 kN and 73.5 kN found by using plastic hinge based beam-column elements and perfect plastic material models, respectively.

As explained before, the Strarch frame is a statically determinate structure during assembly and the stress-erection process. The column at one end of the frame is free to slide horizontally and gap opened. Thus, the value of the axial force of flexible top chord is identical to the tendon force  $t_{ten}$  when the self-weight is ignored during the stress-erection process. Therefore, the required tendon force during stress-erection and the resulting axial force of top chord member are below 90 kN in ideal conditions without considering self-weight. The effect of self-weight in unit Strarch frames can be ignored because of their geometry.

The axial force of 90 kN in the top chord member is a relatively small value when compared to the maximum yielding axial force of  $p_y = A \cdot F_y = 3,430$  kN and the maximum allowable design axial force of 2450kN, both of which are determined by the design method of Strarch frames (Clarke and Hancock 1995, Ket *et al.* 2000). The axial force represents just 2.6% and 3.7% of these values, respectively. Thus, in contrast to the expectations of researchers and engineers, it can be said that the top chord member, on which excessive yield strain is imposed during the stress-erection process, has a sufficient capacity to resist the axial load.

The experimental deformed shape and closed gap shape results are shown in Figs. 10, 11 and 12 show the uniaxial strains at (a), (b), (c), (d), (e) and (f) located at the top and bottom filaments of the section, as illustrated in Fig. 5(a). They show good agreement with the experimental and numerical results for the strain. The strains at locations (e) and (f) near joint exceed the yield strain  $\kappa_0 = 2.437 \times 10^{-03}$ , but

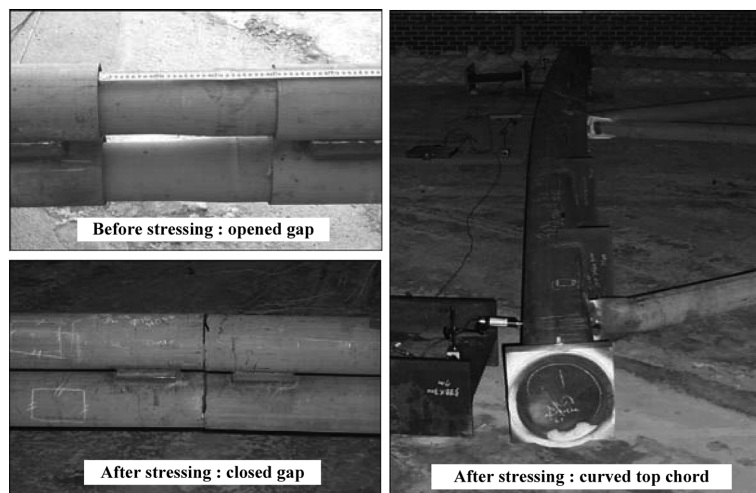


Fig. 10 Closed gap and deformed unit frame: experimental results

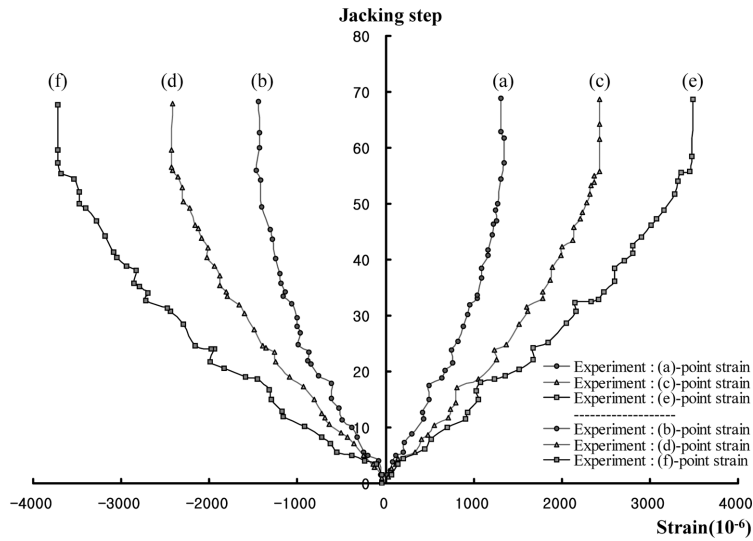


Fig. 11 Uniaxial strain during the stress-erection process: experimental results

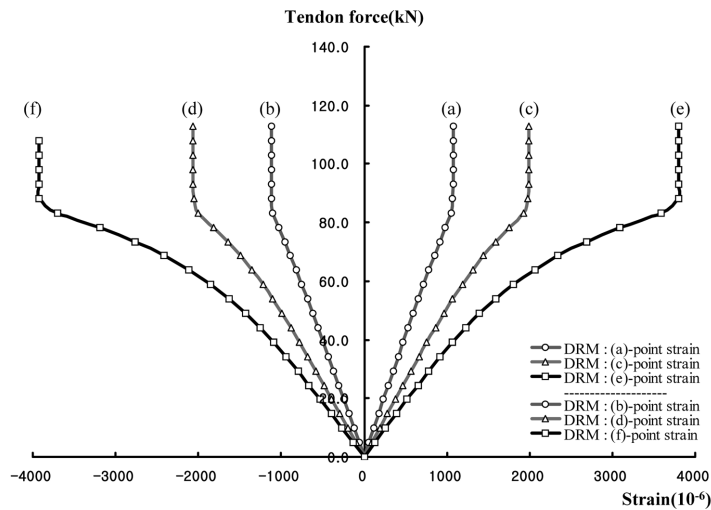


Fig. 12 Uniaxial strain during the stress-erection process: numerical results (Ramberg-Osgood model)

the others for each case of experiment and numerical approach. Therefore, it can be observed that the accuracy and advantages of stress-erection are verified in this study by comparing the results with experimental results and simple equations.

### 5. Buckling analysis of the unit starch frame

An experimental study of the ultimate load capacity of stress-erected unit Starch frames was performed as shown in Figs. 13. and 14 illustrates the analytical model used for the numerical study of

the ultimate load capacity. To identify the analytical and experimental model, one end of top chord is restrained to the displacement and the other end is loaded incrementally. The initial imperfections of curvature and yield strain are considered simultaneously by using the model of stress-erection process analysis of Fig. 7.

As shown in Fig. 15, the ultimate load capacity of the unit Starch frame was determined to be 4018 kN in the experimental study. The design member capacity stated as the lower bound was

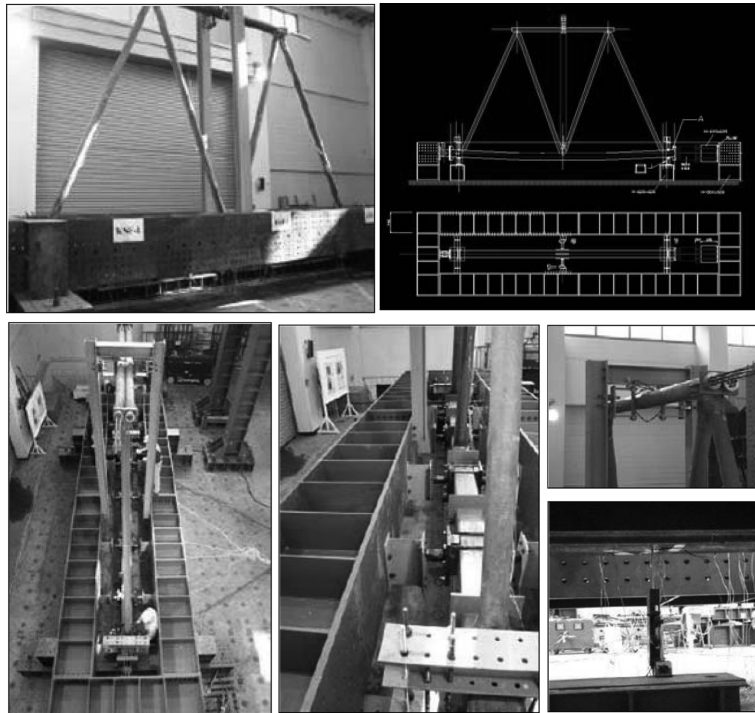


Fig. 13 Experimental study of the ultimate load capacity of unit Starch frames

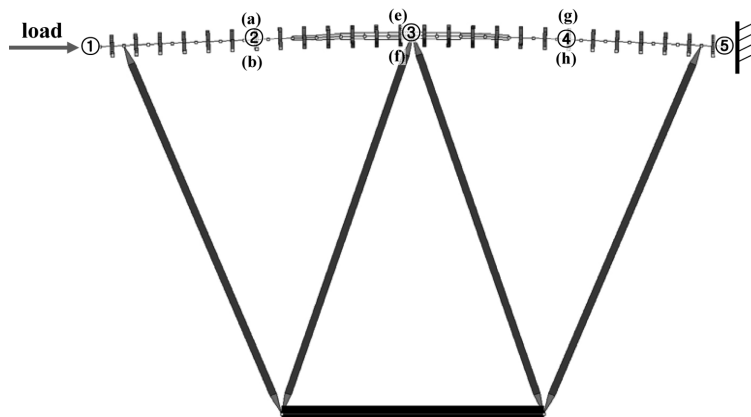


Fig. 14 Analytical model of ultimate load capacity of unit Starch frame with initial imperfections of stress erection

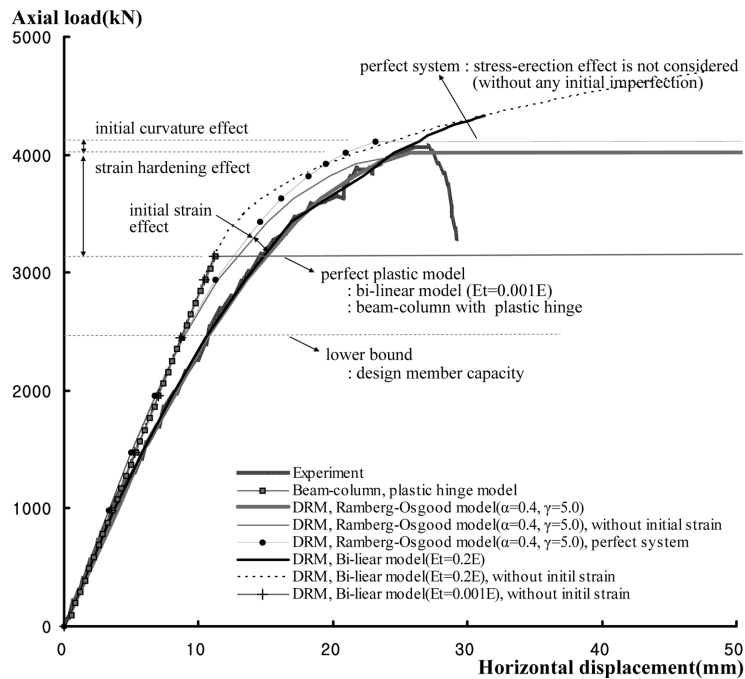


Fig. 15 Load-displacement curves for the ultimate load capacity analysis

calculated to be 2450 kN by using the design curve proposed by Clarke and Hancock (1995). As a result, the safety factor of the unit Starch frame was found to be 1.64 and is a reasonable result for safety of the member design methodology of Starch systems. The allowable axial force of the top chord member leveled out at 60% of the ultimate load capacity.

When strain hardening and initial imperfection effects are considered in the Ramberg-Osgood material models with  $\alpha = 0.4$  and  $\gamma = 5.0$ , the numerical results for the load-displacement curve show good agreement with the experimental results, as illustrated in Fig. 15. When the initial strain is not considered, the load-displacement curve shows more hardening, but an identical ultimate load capacity is calculated. Furthermore, the load-displacement curve of a perfect system, in which the stress-erection effects of the initial curvature and yield strain are not considered, shows a small increase of 2.4% in the ultimate load capacity. As a result, the initial imperfections of curvature and yield strain did not have a significant effect on the strength of the Starch system, contrary to expectation.

In general, the initial imperfections decrease the strength of the structure according to the magnitude of the imperfections. As discussed in Eq. (28) and Fig. 6, the axial force of the top chord induced by the stress-erection process is approximately 90 kN, just 2.2% of the ultimate load capacity, because of the statically determinate nature of Starch frames during stress-erection with gaps and sliding supports. These details of the system decrease the effects of initial imperfections for Starch frame. The axial force of 90 kN was an allowable magnitude in the top chord member. After stress-erection and construction are completed, the Starch frame behaves as a plane truss system with restricted rotation. Therefore, the axial force is the main resisting strength against the external load, and a relatively small bending strain occurs as a result.

As shown in Figs. 16 and 17, the maximum deformation and strain occurred at the midpoint of the member at (b), not near joint, where excessive strain occurred during the stress-erection process. The

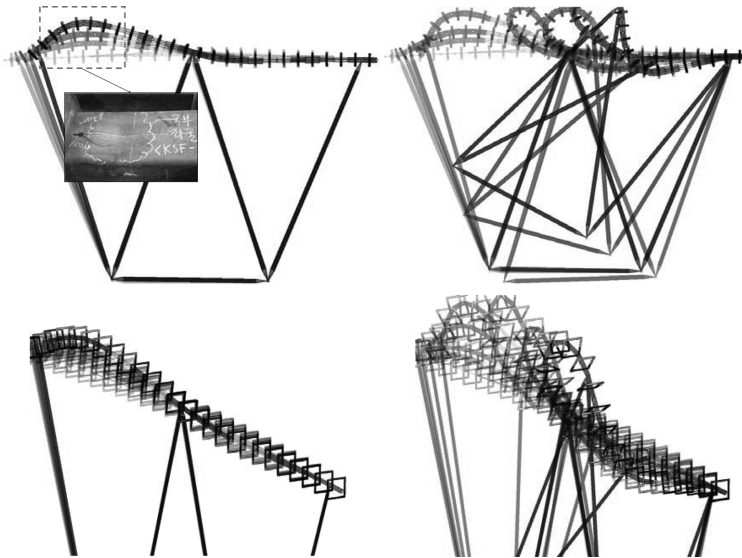


Fig. 16 Buckling and post-buckling shape of the unit Starch frame: Ramberg-Osgood model

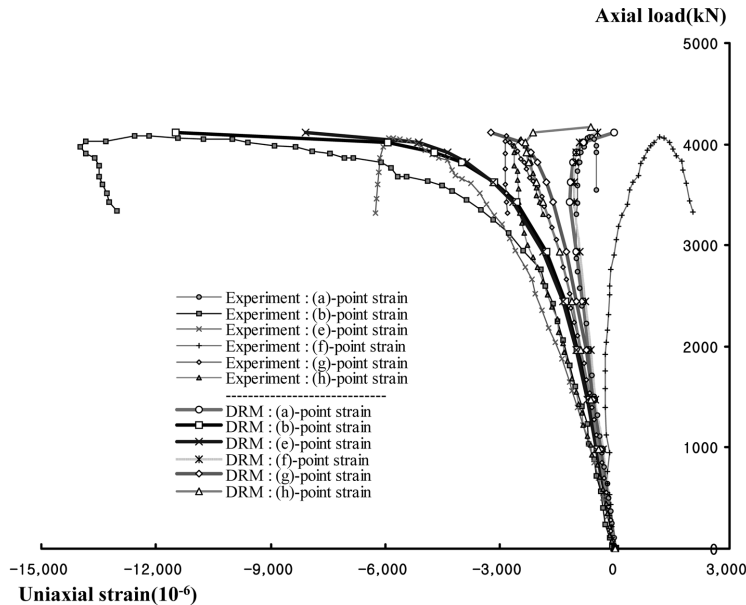


Fig. 17 Uniaxial strain during the ultimate load capacity analysis: Ramberg-Osgood model

critical point at which maximum strain occurs is different in each case. Unlike the stress-erection process, in which a small elastic strain was introduced at this point as shown in Figs. 9, 10 and 11, the maximum strain occurred at (b), the bottom plate of the top chord member, in both the experimental and numerical results. In fact, the local buckling also occurred at this point in previous experimental studies. It can be concluded that the initial strain at (b) has little effect on the axial strength of the unit Starch frame due to the different critical points in the elements.

When the perfect plastic material model (bilinear,  $E_t = 0.001E$ ) and beam column with plastic hinge model are used for buckling analysis without considering strain hardening and initial strain effects, the sudden material failure occurred at point (b) with an axial load value of 3136 kN. This maximum load is approximately 80% of the ultimate load capacity. It can be concluded that the 20% difference in value is due to the strain hardening effect of steel.

The simulation of post-buckling analysis was performed successfully and easily using the explicit numerical method, as shown in Fig. 16. It enabled an analysis without any difficulties caused by numerical instability. When the implicit NR method is used, if the section is arrived at the material failure, the instability of the tangent stiffness matrix during material failure causes the analysis to jump and diverge, causing an unexpected result. Therefore, the progressive post-buckling deformed shape and structural behavior shown in Fig. 16 could not be simulated properly using this method. However, a large amount of effort is required for an analysis of subdivided filament elements and of the DRM, the explicit numerical method. The required iteration is relatively less effective than the stiffness-based implicit method. In spite of this disadvantage, the simplicity and applicability of this study may overcome the disadvantages associated with the numerical algorithm.

## 6. Conclusions

This paper discusses numerical studies of the structural characteristics of Starch systems. The unique features of the stress-erection process are evaluated and the ultimate load capacity analysis is performed considering the initial imperfection effects of the stress-erection process in unit Starch frames. The explicit DRM and displacement-based filament beam elements, in which the section is subdivided into sub-areas of filaments or fibers, are used for the numerical analysis. By using this explicit algorithm, the results of the stress-erection and ultimate load capacity of unit Starch frames are verified by comparison with experimental results.

Using numerical methods, the stress-erection process are analyzed according to various material models and element formulations. The results are verified by comparison with current and past experiments and analytical equations, with which they showed good agreement.

The initial imperfections of curvature and yield strain are introduced into the top chord member. Ultimate load capacity, buckling and post-buckling analyses are performed according to the initial imperfection effects, and through a comparison with the experimental results, it is shown that these initial imperfections induced by the stress-erection process have no significant effect on the strength of unit Starch frames.

## Acknowledgement

This work was supported by the National Research Foundation of Korea (NRF) grant funded by the Korea government (MEST) (No. 2012R1A2A2A01043088) and also supported by the Basic Science Research Program through the National Research Foundation of Korea (NRF) funded by the Ministry of Education, Science and Technology (No. 2012008109).

## Reference

- Alamatian, J. (2012), "A new formulation for fictitious mass of the Dynamic Relaxation method with kinetic damping", *Comput. Struct.*, **90-91**, 42-54.
- Barnes, M.R. (1988), "Form-finding and Analysis of Prestressed Nets and Membranes", *Comput. Struct.*, **30**(3), 685-695.
- Clarke, M.J. and Hancock, G.J. (1995), "Design of Top Chord of Stressed-Arch Frames", *J. Struct. Eng.*, **121**(2), 201-213.
- Day, A.S. (1965), "An introduction to dynamic relaxation", *The Eng.*, **219**, 218-221.
- Han, S.E. and Lee, K.S. (2003), "A Study of the Stabilizing Process of Unstable Structures", *Comput. Struct.* **81**, 1677-1688.
- Jiang, X.M., Chen, H. and Liew, J.Y.R. (2002), "Spread-of-plasticity analysis of three-dimensional steel frames", *J. Constr. Steel Res.*, **58**(2), 193-212.
- Key, P.W., Murray, C.M. and Hwang, K.P. (2000), "The STRARCH STressed-ARCH Building System From Concept To Application", *Sixth Asian Pacific Conference on Shell and Spatial Structures*, 363-370.
- Lee, K.S., Han, S.E. and Park, T. (2011), "A simple explicit arc-length method using the dynamic relaxation method with kinetic damping", *Comput. Struct.*, **89**(1-2), 216-233.
- Lee, K.S. and Han, S.E. (2011a), "Geodesic shape finding of membrane structure with geodesic string by the dynamic relaxation method", *Struct. Eng. and Mech.*, **39**(1), 93-113.
- Lee, K.S. and Han, S.E. (2011b), "Semi-Rigid Elasto-Plastic Post Buckling Analysis of a Space Frame with Finite Rotation", *Int. J. Adv. Steel Constr.*, **7**(3), 275-303.
- Lee, K.S. and Han, S.E. (2011c), "Explicit Stress-Erection and Ultimate Load Analysis of Unit STRARCH Frame Considering Geometrically and Materially Nonlinear Characteristics", *J. Korean Soc. Steel Constr.*, **24**(4), 429-438.
- Lin, S.S. (1997), "Use of Filamented Beam Elements for Bored Pile Analysis", *J. Struct. Eng., ASCE*, **123**(9), 1236-1244.
- Mari, A.R., Bairan, J.M. and Duarte, N. (2010), "Long-term deflections in cracked reinforced concrete flexural members", *Eng. Struct.*, **32**(3), 829-842.
- Rezaiee-Pajand, M. and Alamatian, J. (2010), "The dynamic relaxation method using new formulation for fictitious mass and damping", *Struct. Eng. and Mech.*, **34**(1), 109-133.
- Rezaiee-Pajand, M. and Sarafrazi, S.R. (2010), "Nonlinear structural analysis using dynamic relaxation method with improved convergence rate". *Int. J. Computational Methods*, **7**(4), 1-28.
- Rezaiee-Pajand, M. and Alamatian, J. (2011), "Automatic DR Structural Analysis of Snap-Through and Snap-Back Using Optimized Load Increments". *J. Struct. Eng., ASCE*, **137**(1), 109-116.
- Rezaiee-Pajand, M., Kadhodayan, M., Alamatian, J. and Zhang, L.C. (2011), "A new method of fictitious viscous damping determination for the dynamic relaxation method", *Comput. Struct.*, **89**(9-10), 783-794.
- Rodriguez, J., Rio, G., Cadou, J.M. and Troufflard, J. (2011), "Numerical study of dynamic relaxation with kinetic damping applied to inflatable fabric structures with extensions for 3D solid element and non-linear behavior", *Thin-Walled Struct.*, **49**(11), 1468-1474.
- Topping, B.H.V. and Iványi P. (2007), *Computer Aided Design of Cable-membrane Structures*, Saxe-Coburg Publications.